Imposing Resolved Turbulence by an Actuator in a Detached Eddy Simulation of an Airfoil

Gilling, Lasse; Sørensen, Niels N.; Rethore, Pierre-Elouan Mikael

Published in:
EWEC 2009 Proceedings online

Publication date:
2009

Document Version
Publisher's PDF, also known as Version of record

Imposing Resolved Turbulence by an Actuator in a Detached Eddy Simulation of an Airfoil

Lasse Gilling[*†] Niels N. Sørensen[‡] and Pierre-Elouan Réthoré[*‡]

Abstract

A method is proposed to reduce the computational costs of resolving the incoming freestream turbulence in a detached eddy simulation of an airfoil. The idea is to impose the turbulence directly upstream of the airfoil by an actuator instead of prescribing a fluctuating velocity field at the inlet. Thereby, the mesh upstream of the actuator does not have to resolve the turbulence, and the requirement for mesh resolution is heavily reduced. The method is described and validated as it is shown that the resolved part of the turbulence can be recreated by the actuator. The method is applied to an airfoil flow and it is shown that the results are similar to the approach of imposing the turbulence at the inlet. In the present case the application of the actuator makes it possible to reduce the total number of cells by approximately 60% without coarsening the mesh close to the airfoil.

Keywords: Actuator, Freestream resolved turbulence, Forcing, Airfoil, Detached Eddy Simulation

1 Introduction

In previous work the effect of resolving the inflow turbulence in detached eddy simulations (DES) was studied, c.f. Gilling et al. (2009). It was shown that for the analyzed NACA 0015 airfoil the agreement with experimental results was improved when the inflow turbulence was resolved.

The inflow turbulence was imposed as a fluctuating velocity field on the inlet boundary as was also done by Bechmann (2006). From there the turbulence was convected downstream with the mean velocity. Some distance downstream of the inlet boundary the turbulence met the airfoil and interfered with the boundary layer.

To resolve the turbulence as it was convected from the inlet to the airfoil, the domain upstream of the airfoil was resolved by small cubic blocks. The fine resolution used in the entire domain caused the number of cells to be high (approx. 21 million), and thereby caused a high computational cost of the simulations.

Piomelli (2008) has an overview of different techniques of imposing turbulence on the computational domain in a large eddy simulation. Troldborg (2008) used an actuator to impose a turbulence field upstream of wind turbines (also modeled as actuators). This approach was also used by Spille-Kohof and Kaltenbach (2001) and tested by Keating et al. (2004) for imposing the turbulence in the sheared boundary layer. Here, synthetic turbulence was imposed on the inlet boundary and then they applied forces to amplify the wall normal fluctuations to match some target Reynolds shear-stress.

In this work the turbulence will be imposed directly upstream of the airfoil by using an actuator. Forces are applied in a plane of cells as was done in the work of Troldborg (2008). The forces are chosen to give a desired turbulence field some distance downstream of the actuator. By using this method the domain upstream of the actuator can be resolved by a coarse grid as only the steady mean flow has to be resolved here. This leads to a great saving in the required number of cells.

In this paper the method for generating the turbulence will be described along with the used numerical methods. The methods are verified and calibrated before an example of an airfoil simulation is shown. Finally, some concluding remarks are given.

[*] Aalborg University, Department of Civil Engineering, Sohngaardsholmsvej 57, 9000 Aalborg, Denmark

[†] Tel.: +45 99408544, E-mail: lg@civil.aau.dk

[‡] National Laboratory for Sustainable Energy, Risø-DTU, Technical University of Denmark, Wind Energy Division, Frederiksborgvej 399, P.O. Box 49, 4000 Roskilde, Denmark

2 Method

An actuator is used to prescribe some given velocity change. In Figure 1 the pressure jump and the velocity change at an actuator is shown. The fluid is accelerated from U_∞ to $U_\infty + \Delta u$ by the pressure jump. The pressure required to accelerate the flow is, Hansen (2008)

$$\Delta p = \frac{1}{2}\rho\left((U_\infty + \Delta u)^2 - U_\infty^2\right) \tag{1}$$

where ρ is the density of the fluid. The pressure is derived from steady one-dimensional momentum theory using the Bernoulli equation.

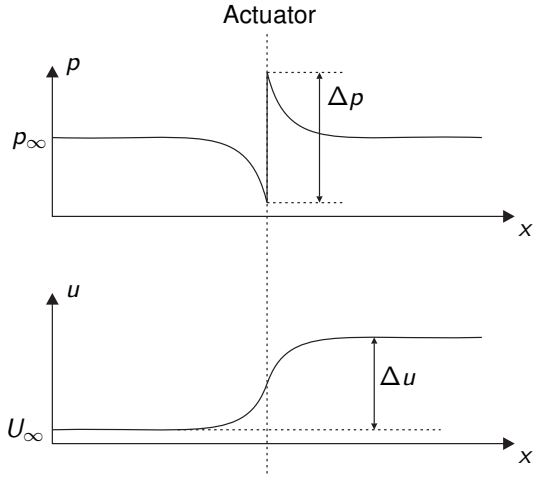

Figure 1: Pressure jump at the actuator and change of velocity at the actuator (dashed line).

The pressure jump corresponds to a force applied in each computational cell crossed by the actuator. The magnitude of these forces is

$$F_c = \frac{1}{2}\rho A_c\left(U_\infty + \frac{1}{2}\Delta u\right)\Delta u \tag{2}$$

where A_c is the area of the disc crossed by the cell. This can be generalized to include velocity changes in three dimensions

$$\mathbf{F}_c = \frac{1}{2}\rho A_c\left(U_\infty + \frac{1}{2}\Delta u\right)\Delta \mathbf{u} \tag{3}$$

where **u** and **F** are vectors containing the three components of velocity and force vectors, respectively. The forces are imposed in the cells using the method described by Réthoré and Sørensen (2008).

The above derivation is based on a steady state consideration. When applying a fluctuating velocity field this steady state consideration is not valid. However, the obtained velocity field is in good agreement with the target velocity field, as will be shown in Section 4.

3 Numerical Methods

The incompressible Navier-Stokes equations are solved using EllipSys3D by Sørensen (1995) and Michelsen (1992, 1994). It is a structured, finite volume CFD-code developed at RISØ and Technical University of Denmark. The PISO-algorithm is used to enforce the pressure-velocity coupling. A modified version (c.f. Réthoré and Sørensen (2008)) of the Rhie-Chow pressure correction algorithm is used to avoid odd-even pressure decoupling and numerical wiggles at the actuator. The momentum equations are solved with the 4th order central difference scheme and a 2nd order accurate time stepping algorithm is used. The simulations are DES as proposed by Spalart et al. (1997), but also the incoming freestream turbulence is resolved. The $k-\omega$ SST subgrid model by Menter (1993) is used.

4 Verification

In the present section the method's ability to generate a chosen turbulence field is demonstrated. The computational domain is shown in Figure 2. It consists of $192 \times 192 \times 128$ cells in the x, y and z directions, respectively. The physical dimensions are approximately $12L \times 12L \times 6L$ where L is the integral length scale of the turbulence.

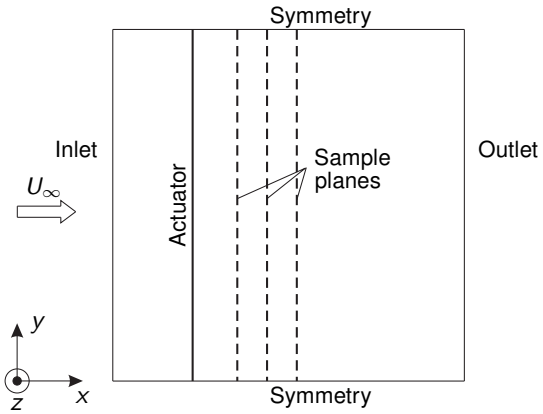

Figure 2: The computational domain.

The imposed turbulence is generated by the method of Mann (1998), and has been run through a precursor simulation. Thereby, the turbulence has adapted to the computational mesh and the numerical method, and any flaws in the synthetic field has been corrected by the Navier-Stokes solver. The average resolved kinetic energy is $10^{-3}U_\infty^2$ giving a turbulence intensity of 2.6%. The CFL number based on the mean velocity is 0.25.

The turbulence is sampled in a number of planes downstream of the actuator. The sampled time series are compared to the time series from the precursor to show that the resolved turbulence can be recreated by the actuator. In Figure 3 the ratios of standard deviations and the correlation coefficient are shown.

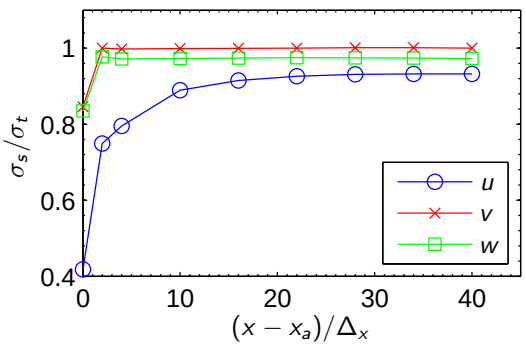

(a) Ratios of sampled to target standard deviation.

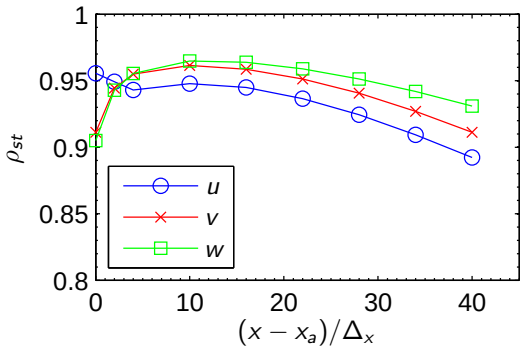

(b) Average correlation coefficient between sampled and target time series.

Figure 3: Comparison between sampled and target time series of turbulence as function of distance from the actuator. The distance is measured in number of cells.

It is seen that the resolved turbulence sampled downstream of the actuator is very similar to the target turbulence field from the precursor. The ratios of standard deviations are measures of the energy content compared to the target turbulence. The energy in the transverse directions is generated almost directly at the actuator. The energy on the streamwise component builds up slowly over the first 30 to 40 cells. The obtained ratios are 0.93, 1.00 and 0.98 for the u, v and w components, respectively.

The correlation coefficients in Figure 3(b) show that the generated turbulence is highly correlated with the target turbulence field. The correlation peaks at $95-97\%$ around 10 cells downstream of the actuator.

In conclusion the generated field is very similar to the target turbulence field, but it contains about 7% too little energy on the streamwise component. This deficiency can be corrected by the introduction of a vector of constants $\mathbf{G}$ in (3)

$$\mathbf{F}_c = \frac{1}{2}\mathbf{G}\rho A_c \left(U_\infty + \frac{1}{2}\Delta u \right) \Delta \mathbf{u} \tag{4}$$

which should be evaluated component by component. $\mathbf{G} = [1.07, 1.00, 1.02]$ has been chosen to give unitary ratios of the standard deviations. The result of this modification is shown in Figure 4.

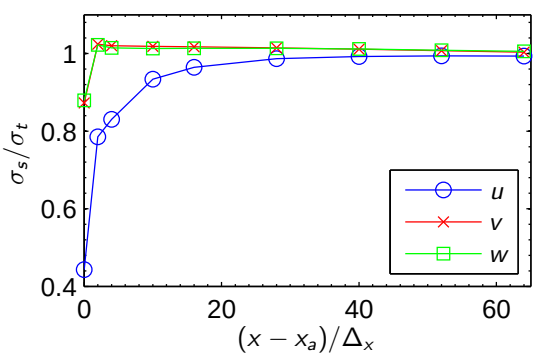

(a) Ratio of sampled to target standard deviation.

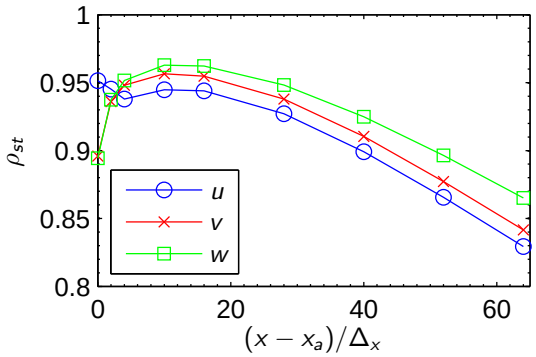

(b) Averaged correlation coefficient between sampled and target time series.

Figure 4: Comparison between sampled and target time series. The modified (4) is used.

The standard deviations of the sampled field are now within 1% of the standard deviations of the target turbulence field. Through several simulations a value of $\mathbf{G}$ in the order of $[1.1, 1.0, 1.0]$ has been found be be appropriate. An investigation has shown the constant to be independent from the mesh resolution, the turbulence intensity, the freestream velocity, the CFL number, the difference scheme, the number of subiterations and the relaxation coefficients.

In Figure 5 the samples of time series of the u and v components are shown. The modified forces, eq. (4), are used and the time series are sampled 10 cells downstream of the actuator.

The spatial decay of homogenous, isotropic turbulence has briefly been studied. Using the actuator approach, the turbulence appears to decay too slow compared to an empirical expression. For the present application it is considered to be of no importance; the decay is very low in any case on the time scales comparable to a chord passage.

The turbulence imposed here has been sampled from a precursor simulation. Synthetic turbulence from the method of Mann (1998) has also been imposed directly. In this case the turbulence generated by the actuator corresponds to a low-pass filtered version of the synthetic turbulence. The filtering is caused by the limited ability to resolve the smallest eddies in the simulations.

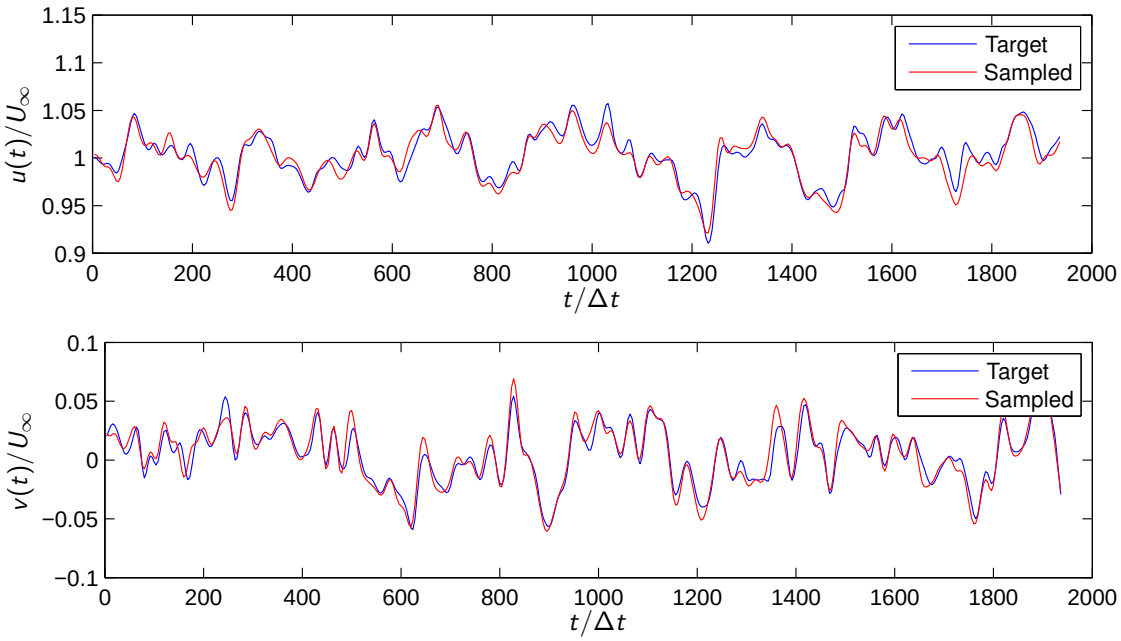

Figure 5: Sampled and target time series.

5 Example: Airfoil in Turbulent Inflow

An actuator is used to impose the resolved turbulence upstream of an airfoil in a DES. The airfoil is a NACA 0015 profile and the Reynolds number is 1.6 million. The angle of attack is 16°. The freestream turbulence intensity is 2% and the integral length scale is 0.25 chords, which have been found to give good agreement with the experimental results of Bove (2008). The results are compared to a simulation where the inflow turbulence is imposed as a fluctuating inflow boundary condition, c.f. Gilling et al. (2009).

5.1 Numerical Setup

The mesh used in the simulation is shown in Figure 6. The geometry is chosen to match the geometry of the LM wind tunnel like in Gilling et al. (2009). However, the number of cells is reduced from about 21 million to 6.8 million. The reduction is primarily obtained because the freestream turbulence is now imposed directly upstream of the airfoil. Thereby the mesh upstream of the actuator can be much coarser, as only the steady mean flow has to be resolved here. About 4.7 million cells have been saved using a lower resolution in the downstream domain, but the remaining 9.4 million cells saved is a direct consequence of imposing the turbulence by an actuator.

The inlet is located about four chords upstream of the airfoil and the outlet approximately 25 chords downstream. The top and bottom boundary conditions are chosen to be symmetry to limit the flow without having to resolve the boundary layer at a wall. For the same reason the periodicity is chosen in the spanwise direction. The actuator is located 0.8 chords upstream of the leading edge of the airfoil.

The O-mesh close to the airfoil is generated using the code described in Sørensen (1998). The O-mesh is identical to that of Gilling et al. (2009), and so is the mesh spacing directly up- and downstream of it. Here the cells are close to cubic with a side length about 1.5% of the chord. As shown in Figure 6 the cells up- and downstream of the cubic cells are stretched, with stretching ratios 5 and 10%, respectively. The cells above and below the O-mesh are also stretched slightly to reduce the total number of cells. In summary, the mesh is fine close to the airfoil, where a fine resolution is

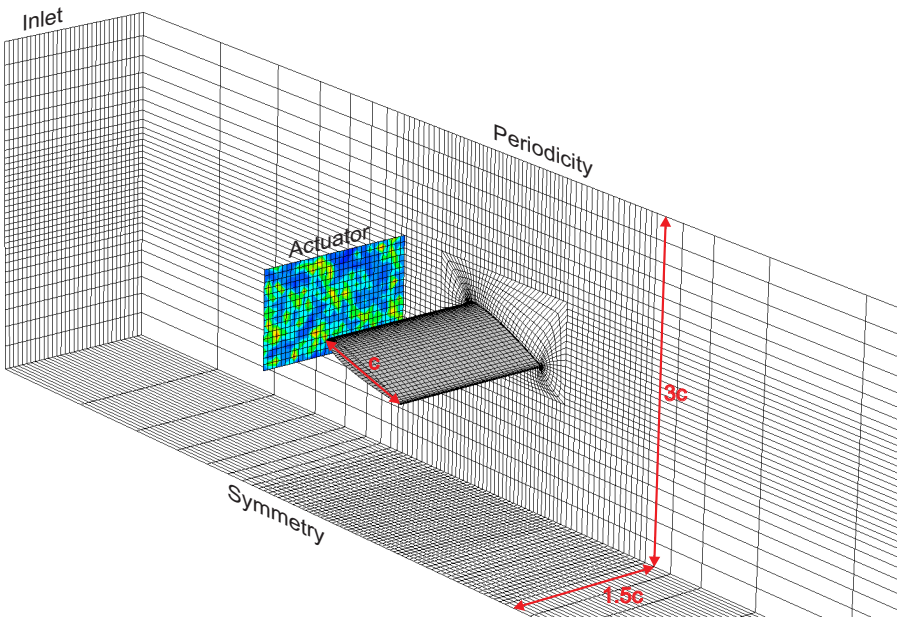

Figure 6: The computational mesh. Every fourth cell is shown.

required to resolve the freestream turbulence and the wake, and everywhere else the resolution is coarser.

5.2 Results and Discussion

In Figure 7 instantaneous contours of vorticity close to the airfoil are shown. The turbulence is seen to enclose the airfoil and follow the induced velocity field. The turbulent structures are warped around the leading edge of the airfoil. It can also be noted that the vorticity is smeared out when the cells are stretched.

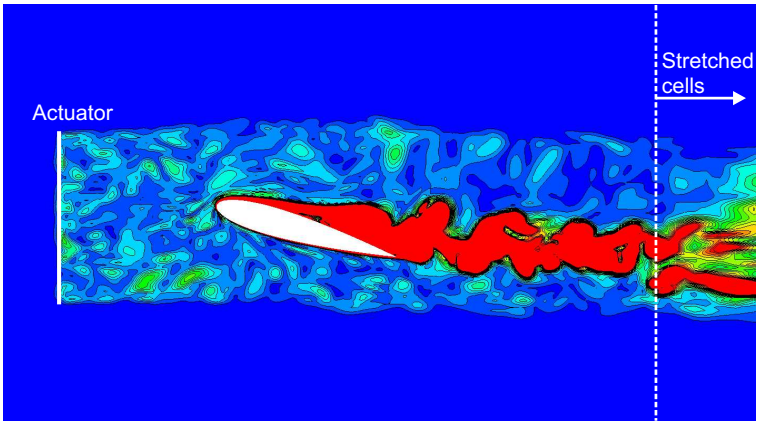

Figure 7: Contours of vorticity close to the airfoil.

To obtain the correct behavior of the subgrid turbulence, care need to be taken when specifying the inflow values of the subgrid turbulence model. From the precursor simulation the level of the eddy viscosity is known. The level of eddy viscosity close to the airfoil is crucial for the prediction of surface pressure. The values of k and ω on the inlet boundary are chosen to give the correct eddy viscosity in the freestream turbulence downstream of the actuator.

In Figure 8 the lift and drag coefficients are shown. The magenta dot shows the present simulation with turbulence imposed by the actuator. It is seen that the flow is stalled at 16°. By comparing to the simulation where the freestream turbulence was imposed as a fluctuating velocity on the inlet the agreement is seen to be in the same order as the experimental scatter. From the other simulations with different turbulence intensities the flow is seen to be very sensitive at this angle of attack.

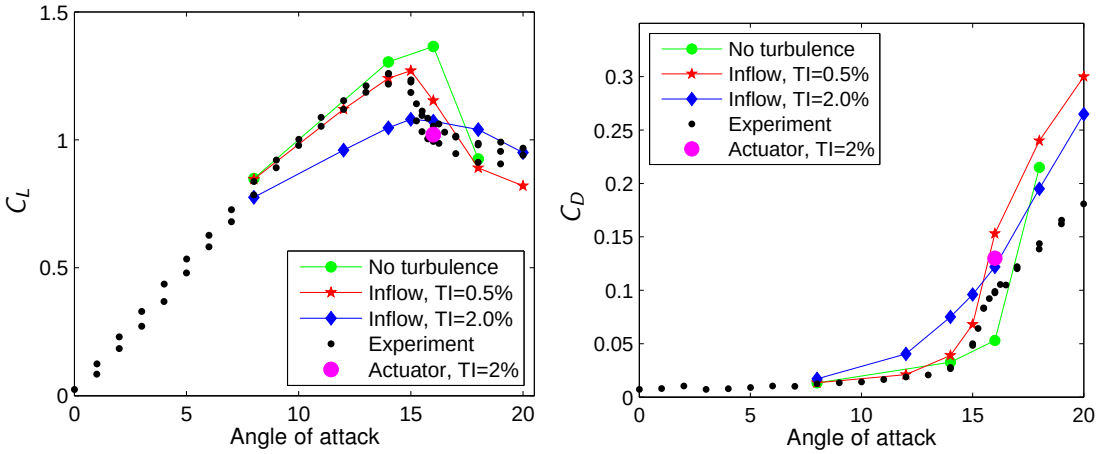

(a) Lift coefficient.

(b) Drag coefficient.

Figure 8: Polar of the NACA 0015 airfoil at a Reynolds number of 1.6 million. The experimental results are from Bove (2008) and the simulated results are from Gilling et al. (2009). The green lines with dots are standard DES without any resolved freestream turbulence. The scatter in the experimental results is caused by the low Reynolds number, for which the measurement system in the wind tunnel is not calibrated.

In Figure 9 the surface pressure and skin friction coefficients are plotted. The results are seen to be very similar to the simulation with turbulence imposed at the inlet. The flow on the suction side is seen to separate slightly less. Similar small differences can probably be observed in simulations with different realizations of the freestream turbulence irrespective of whether it is imposed at the inlet or by an actuator.

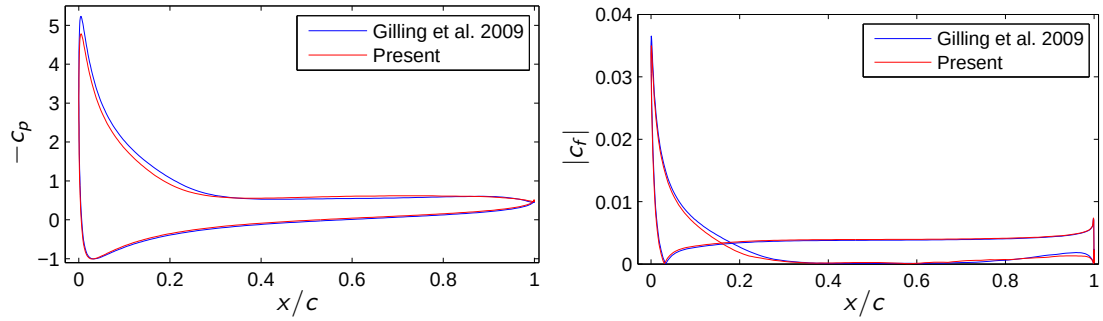

Figure 9: Surface pressure and skin friction coefficient.

6 Conclusions

The actuator is able to recreate the resolved part of the freestream turbulence with good accuracy. The obtained correlation coefficients are about 0.95, and with the introduction of a constant, the energy level of the turbulence is correct as well. The subgrid part of the turbulence is only established slowly.

For the present application it is proposed to choose inflow values of k and ω of the subgrid model to give the correct eddy viscosity in the freestream turbulence downstream of the actuator.

Good results are obtained for the airfoil flow. The results from the turbulence imposed by an actuator are very similar to the results of the simulation with turbulence imposed at the inlet. The applied method shows a large potential as the computational costs can be heavily reduced. Comparing to the previous approach the number of cells is reduced by 60% without coarsening the mesh close to the airfoil. The computational cost using the actuator method is similar to the cost of a standard DES without resolved inflow turbulence.

Acknowledgments

This work was funded by the "Danish Research Council for Strategic Research" under the project "Airfoils in Turbulent Inflow". The simulations were carried out on the Linux cluster Alfheim located at DTU and financed by the "Danish Center for Scientific Computing" under grant nr. HDW-0107-02 from 2007. The experimental data provided by LM Glasfiber is gratefully acknowledged.

References

Bechmann, A. (2006). *Large-Eddy Simulation of Atmospheric Flow over Complex Terrain*. PhD thesis, Risø National Laboratory, Roskilde.

Bove, S. (2008). Lswt report of campaign naca 0015_1. Technical report, LM Glasfiber, Lunderskov.

Gilling, L., Sørensen, N. N., and Davidson, L. (2009). Detached eddy simulations of an airfoil in turbulent inflow. In *47th AIAA Aerospace Sciences Meeting*, Orlando, FL. AIAA paper no. 2009-270.

Hansen, M. O. (2008). *Aerodynamics of Wind Turbines*. Earthscan, London.

Keating, A., Piomelli, U., Balaras, E., and Kaltenbach, H.-J. (2004). A priori and posteriori tests of inflow conditions for large eddy simulations. *Phys. Fluids*, 16:4696–4712.

Mann, J. (1998). Wind field simulation. *Probabilistic Engineering Mechanics*, 13(4):269–282.

Menter, F. R. (1993). Zonal two equation $k-\omega$ turbulence models for aerodynamic flows. In *24th Fluid Dynamics Conference*, AIAA paper no. 93-2906, Orlando, FL.

Michelsen, J. A. (1992). Basis3d - a platform for development of multiblock pde solvers. Technical Report AFM 92-05, Technical University of Denmark, Lyngby.

Michelsen, J. A. (1994). Block structured multigrid solution of 2d and 3d elliptic pdes. Technical Report AFM 94-06, Technical University of Denmark, Lyngby.

Piomelli, U. (2008). *Large Eddy Simulation and Related Techniques: Theory and Applications*, chapter Large-eddy simulation of turbulent flows. von Karman Lecture Series. von Karman Institute for Fluid Dynamics, Rhode-St-Genèse, BE.

Réthoré, P.-E. and Sørensen, N. N. (2008). Actuator disc model using a modified rhie-chow/simple pressure correction algorithm. comparison with analytical solutions. In *EWEC2008*, Brussel, BE.

Sørensen, N. N. (1995). *General Purpose Flow Solver Applied to Flow over Hills*. PhD thesis, RISØ National Laboratory, Roskilde. Risø-R-827(EN).

Spalart, P. R., Jou, W.-H., Strelets, M., and Allmaras, S. R. (1997). Comments on the feasibility of les for wings, and on a hybrid rans/les approach. In Liu, C. and Liu, Z., editors, *1st AFOSR International Conference on DNS/LES*, pages 137–147, Columbus OH. Greyden Press.

Spille-Kohof, A. and Kaltenbach, H.-J. (2001). Generation of turbulent inflow data with a prescribed shear-stress profile. In *NDS/LES Progress and Challenges*, pages 319–326, Columbus, OH. Greyden Press.

Sørensen, N. N. (1998). Hypgrid2d a 2-d mesh generator. Technical Report Risø-R-1035(EN), Risø.

Troldborg, N. (2008). *Actuator Line Modelling of Wind Turbine Wakes*. PhD thesis, Technical University of Denmark, Lyngby.